

## Raman spectra of solid isotopic hydrogen mixtures

B. J. Kozioziemski and G. W. Collins

*Lawrence Livermore National Laboratory, Livermore, California 94551*

(Received 13 November 2002; published 1 May 2003)

Rotational and vibrational Raman spectra are investigated for mixtures of hydrogen isotopes in the solid phase. The  $S_0(0)$  rotational Raman transitions are asymmetrically broadened in energy for each isotope in the mixture compared to their respective pure component transitions. The isotopic energy shift of  $S_0(0)$  breaks the lattice symmetry and limits the roton hopping responsible for the well defined  $S_0(0)$  triplet found in the pure component. The  $S_0(0)$  line shapes of tritiated and nontritiated mixtures are nearly identical, and shows there is little effect from radiation damage. The vibrational  $Q_1(J)$  lines are shifted to higher energy, and the  $Q_1(1)/Q_1(0)$  intensity ratio is decreased in the mixtures relative to the pure component. Both effects are due to a localization of the vibrons in mixtures.

DOI: 10.1103/PhysRevB.67.174101

PACS number(s): 78.30.Hv, 33.20.Vq, 33.20.Fb

### I. INTRODUCTION

Hydrogen forms a molecular quantum solid at low temperatures which has engaged a great deal of interest throughout the last century and continues today. The many research areas studied include anisotropic interactions,<sup>1-4</sup> matrix impurities,<sup>5-7</sup> rotational diffusion,<sup>8</sup> and pressure effects<sup>9-11</sup> on the rotational and vibrational Raman spectra.<sup>8,12,13</sup> Research continues to focus on hydrogen in high pressure and fusion energy research, both of which may use the Raman spectra as a diagnostic. The National Ignition Facility in particular will use an isotope mixture of 25%-50%-25%  $D_2$ -DT- $T_2$  (D-T) in high-gain fuel capsules.<sup>14</sup> The rotational Raman spectrum provides one measurement of the isotope concentrations in the fuel layer.<sup>15,16,17</sup> While the Raman spectra of single isotope hydrogen solids are well known, those of mixtures, particularly with tritium, have received less attention.

Properties of the hydrogen molecules in the zero-pressure solid are not too different from those of the free molecules.<sup>8,13</sup> The weak intermolecular interactions do not mix rotational energy states; hence the rotations are free and  $J$  is a good quantum number.  $\Delta J=2$  is first allowed rotational transition for homonuclear molecules. The fivefold  $J = 2$  degeneracy is lifted and the rotational states are broadened into an energy band by the crystal field interaction. Similarly, the molecular vibrational states are weakly perturbed by the intermolecular interactions, also forming a band in the solid. The rotational and vibrational Raman spectra probe the respective energy bands in the solid.

Radiation damage in D-T results from the beta decay of the triton.<sup>18</sup> The mean decay energy of 5.7 keV goes into ionization, dissociation, molecular excitations, and the heating of the solid. The free atoms created by the beta decay were shown to convert  $J = 1$  molecules as the atoms rapidly hop through the lattice.<sup>19-21</sup> Hence, the  $J = 1$ -to-0 conversion proceeds much faster in D-T than in nontritiated hydrogens. The effect of radiation damage on the rotational and vibrational bands was studied using infrared spectroscopy,<sup>22</sup> but no work has yet explored the Raman spectrum. This paper shows that there is little change in the rotational and vibrational Raman spectra due to tritium radiation damage to

the solid. However, the spectra of the mixtures do differ from those of the pure component hydrogens.

The notation of Souers<sup>18</sup> is followed in this paper, with any of the six diatomic combination of H, D, and T atoms referred to as hydrogen and referring to specific isotopic combinations when required, i.e.,  $H_2$ , HD. H-D will refer to mixtures of  $H_2$ ,  $D_2$ , and HD. The Raman spectrum for the rotational transitions  $S_0(0)$  and  $S_0(1)$  and the vibrational transitions  $Q_1(0)$  and  $Q_1(1)$  of hydrogen relevant to this paper are reviewed first. These results for pure hydrogens provide the basis for understanding the observed spectrum in mixtures. Sections III and IV compare mixtures of H-D and D-T with pure component samples.

#### A. Review of rotational Raman spectrum

Only the rotational  $J = 0$  ground and  $J = 1$  metastable states are populated in the low temperature and pressure solid hydrogens.<sup>8,18</sup> Neighboring  $J = 1$  molecules in  $H_2$ ,  $D_2$ , and  $T_2$  solids interact via their magnetic dipoles (and electric quadrupoles for  $D_2$ ) thus decoupling the nuclear spins and enabling conversion from the metastable  $J = 1$  state to the  $J = 0$  state.<sup>13,23-25</sup> The conversion rate is slow enough to permit treating  $J = 1$  and  $J = 0$  molecules as separate species.  $c(J)$ , the concentration of molecules in rotational state  $J$ , is determined from the  $\Delta J=2$  allowed Raman transitions  $S_0(0)$  and  $S_0(1)$  of the homonuclear molecules as follows. The scattering intensity for  $\Delta J=2$  is calculated to be proportional to the number of molecules in the initial rotational state  $J$ ,  $N(J)$ , according to<sup>15</sup>

$$I_J \propto N(J) \frac{(J+1)(J+2)}{(2J+3)(2J+1)} \omega^4 |\langle \psi | \alpha_J | \psi \rangle|^2. \quad (1)$$

The anisotropic polarizability matrix elements  $\langle \psi | \alpha_{J=0} | \psi \rangle$  and  $\langle \psi | \alpha_{J=1} | \psi \rangle$  differ by less than 1% for  $H_2$  molecules, while the  $H_2$  and  $D_2$  isotope polarizabilities differ by 4%.<sup>26,27</sup> Further, there is no phonon interaction because the rotational transition energies of the hydrogens are larger than their Debye temperatures. Hence,  $N(1)/N(0)$  is obtained from the ratio of the scattering intensities  $I(J = 1-3)/I(J = 0-2)$  as<sup>16</sup>

$$\frac{N(J=1)}{N(J=0)} = \frac{5}{3} \frac{I(J=1-3)}{I(J=0-2)}. \quad (2)$$

The isotopic concentrations in hydrogen mixtures are obtained from the Raman intensities by scaling appropriately according to the anisotropic polarizabilities.<sup>27</sup> Thus, the rotational Raman spectrum provides the concentrations of the isotopes and rotational states.

The electric quadrupole-quadrupole (EQQ) and crystal field interactions in the solid couple hydrogen molecules and partially lift the degeneracy of the five  $m_J$   $S_0(0)$  transitions. The resulting Raman spectrum is a well defined triplet (doublet) for pure  $H_2$  or  $D_2$  with less than  $c(1) = 5-10\%$  in the hcp (fcc) lattice.<sup>8,10,28</sup> Both interactions are reviewed, since they provide a basis for understanding the Raman spectrum of hydrogen mixtures.

### 1. EQQ interaction

The EQQ interaction couples the  $J = 2$  excitation to neighboring  $J = 0$  molecules, enabling the excitation to hop through the lattice. A rotational exciton band results, with the allowed energies dependent on the lattice structure. Van Kranendonk provided a solution to both the fcc and hcp lattices using Bloch's theorem. The allowed energy states  $E(\mathbf{k})$  with roton waqve function amplitude  $A_m(\mathbf{k})$  of the hcp lattice are the solutions to the  $10 \times 10$  secular equation [Eq. (4.43) in Ref. 8]

$$\sum_n H_{m,n}(\mathbf{k}) A_n(\mathbf{k}) = E(\mathbf{k}) A_m(\mathbf{k}). \quad (3)$$

The fcc expression is similar and not presented here. The Hamiltonian matrix is defined as

$$H_{m,n} = \sum_j \langle 2m, R_i | V_{EQQ} | 2n, R_j \rangle = \epsilon_{02} c_{mn} S_{n-m}, \quad (4)$$

where  $\epsilon_{02}$  is the quadrupole coupling constant and  $c_{mn} = \sqrt{70}(-1)^m C(224; m\bar{n})$  incorporates the Clebsch-Gordon coefficient.  $R_i$  is the position of the  $i$ th molecule. The lattice sums are expressed as

$$S_\mu = \sum_\rho \left( \frac{R_0}{R_\rho} \right)^5 C_{4\mu}(\Omega_\rho), \quad (5)$$

where  $C_{4\mu}(\Omega)$  is the Racah spherical harmonic,  $R_\rho$  and  $\Omega_\rho$  are the distance and angle to the molecular site  $\rho$ , and  $R_0$  is the nearest neighbor separation. The point symmetry of the hcp lattice makes the lattice sum nonzero only when  $\mu = 0$ . The approximation of  $\mathbf{k} = 0$  is made in Eq. (3) since the wave vector of the excitation is small compared to the lattice spacing. The eigenvalues of Eq. (3) are the five Raman allowed energy states that have three distinct energies,  $0.903\epsilon_{02}a_m(4)$ , where  $a_{\pm 1} = -4$ ,  $a_{\pm 2} = 1$ , and  $a_0 = 6$ , and the factor of 0.903 is the resulting value of the lattice sum.<sup>8</sup> Hence, the rotational spectrum in a hcp lattice consists of three equally spaced lines. The above derivation assumes a

rigid lattice, with the details of phonon renormalization available.<sup>8</sup> Crystal field interactions modify the above energies as described below.

### 2. Crystal field terms

The crystal field terms are due to the interaction of the anisotropic potential of the  $J = 2$  molecule with the isotropic part of the neighboring  $J = 0$  molecules. The potential is expressed in the crystal reference frame with the  $z$  axis along the hexagonal  $c$  axis as<sup>1</sup>

$$V_c = \sum_{\substack{l=2,4 \\ n=-l,l}} \epsilon_{ln} Y_{ln}(\omega), \quad (6)$$

where  $\omega$  is the orientation of the molecule in the hcp lattice,  $Y_{ln}$  is the spherical harmonic, and the coupling constants are given by<sup>1</sup>

$$\epsilon_{ln} = \sum_i g(R_i) Y_{ln}^*(\alpha_i, \beta_i). \quad (7)$$

Here,  $g(R_i)$  is the radial part of the potential,  $R_i$ ,  $\alpha_i$  and  $\beta_i$  refer to the coordinates of the central  $J = 2$  molecule pointing to the neighboring  $J = 0$  molecules, and the sum is over all molecules in the crystal. All of the  $n \neq 0$  terms are zero due to the point symmetry of the single component hcp lattice, and  $|2m\rangle$  states are not mixed.

For any given configuration of  $H_2$  or  $D_2$  molecules in the lattice the crystal field energies can be calculated by diagonalizing the potential according to

$$E = \langle 2m | V_c | 2m \rangle. \quad (8)$$

The sum in Eq. (7) drops off quickly with  $R_i$  and only the first few shells of neighbors need be considered. The solution for the crystal field energies are<sup>29</sup>

$$E_c(2m) = -\frac{2}{7} c_m \epsilon_{2c} + \frac{1}{21} a_m \epsilon_{4c}, \quad (9)$$

where  $a_m$  are as defined for the EQQ interaction and  $c_{\pm 2} = 1$ ,  $c_{\pm 1} = -1/2$ ,  $c_0 = -1$ . Hence, a non-zero  $\epsilon_{2c}$  leads to unequal values of  $\Delta_1 = S_0(0)_{\pm 2} - S_0(0)_{\pm 1}$  and  $\Delta_2 = S_0(0)_0 - S_0(0)_{\pm 2}$ . The measured difference of  $\Delta_1$  and  $\Delta_2$  originally measured by Bhatnagar<sup>30</sup> is  $0.03 \text{ cm}^{-1}$  for  $H_2$ , small compared to  $\Delta_1 = 2.01 \text{ cm}^{-1}$ . This early measurement is consistent with more recent high resolution methods.<sup>31,32</sup> The  $\epsilon_{4c}$  term has the same symmetry as the EQQ interaction, but is negative in sign.<sup>29</sup> Hence, the triplet spacing is reduced from the EQQ hopping calculation.

The above results are valid for hydrogens with  $c(1)$  less than a few percent. The  $S_0(0)$  line is broadened and the triplet is unresolvable above  $c(1) = 20\%$  in  $D_2$ .<sup>30</sup> In contrast, Hardy *et al.*<sup>16</sup> studied the rotational Raman spectrum of  $H_2$  and  $D_2$  with very low  $c(0)$  in a  $J = 1$  lattice. In this case,  $J = 0$  molecules are the impurities. They found the  $S_0(0)$   $m_J$  energies, listed in Table I, were consistent with the  $Pa3$  lattice symmetry for the the ordered lattice at 1.16 K, with an ordering of the  $m_J$  components that differs from the hcp lattice. However, the  $S_0(0)$  line is broad and asymmetric in

TABLE I. Solid phase  $S_0(0)$  energies. The first nine are measured in this work while the last four provide reference values.  $m_J$  are identified only when known.

Isotope	Composition	Position ( $\text{cm}^{-1}$ )	FWHM ( $\text{cm}^{-1}$ )	Splitting ( $\text{cm}^{-1}$ )	%J=1	Temp. (K)
H <sub>2</sub>	12% H <sub>2</sub> -88% D <sub>2</sub>	352.8	3.0		<5	8.5
		355.3	1.8	2.5		
		357.9	3.4	2.6		
D <sub>2</sub>	100% D <sub>2</sub>	$m_{\pm 1} = 177.1$	1.0		<1	12.5
		$m_{\pm 2} = 179.6$	1.0	2.5		
		$m_0 = 182.1$	1.0	2.5		
D <sub>2</sub>	12% H <sub>2</sub> -88% D <sub>2</sub>	177.4	2.9		<5	8.5
		179.8	2.5	2.4		
		182.3	2.5	2.5		
D <sub>2</sub>	23% H <sub>2</sub> -77% D <sub>2</sub>	177.4	4.1		<5	8.5
		180.0	3.8	2.6		
		182.3	3.8	2.3		
D <sub>2</sub>	77% H <sub>2</sub> -23% D <sub>2</sub>	177.2	3.0		<5	9.2
		179.5	1.3	2.25		
		182.2	3.8	2.7		
D <sub>2</sub>	46% H <sub>2</sub> -38% HD-16% D <sub>2</sub>	176.5	2.9		<5	7.5
		178.8	1.1	2.3		
		181.8	2.9	3.0		
D <sub>2</sub>	29% H <sub>2</sub> -51% HD-20% D <sub>2</sub>	176.1	2.6		<5	8.0
		178.4	1.4	2.3		
		181.8	3.5	3.4		
D <sub>2</sub>	D-T	CM - 178.8			<2	10.2
		peak - 176.8				
T <sub>2</sub>	D-T	116.3	2.2		<2	10.2
		118.8	2.2	2.5		
		122.7	4.2	3.9		
H <sub>2</sub> (Bhatnagar <i>et al.</i> ) (Ref. 30)	100% H <sub>2</sub>	$m_{\pm 1} = 351.84$	0.6		<1	2
		$m_{\pm 2} = 353.85$	0.6	2.01		
		$m_0 = 355.83$	0.6	1.98		
D <sub>2</sub> (Bhatnagar <i>et al.</i> ) (Ref. 30)	100% D <sub>2</sub>	$m_{\pm 1} = 176.8$	2		20	2
		$m_{\pm 2} = 179.4$	2	2.6		
		$m_0 = 182.0$	2	2.6		
D <sub>2</sub> (McTague <i>et al.</i> ) (Ref. 34)	100% D <sub>2</sub>	$m_{\pm 1} = 176.61$			2	?
		$m_{\pm 2} = 179.17$		2.56		
		$m_0 = 181.75$		2.58		
D <sub>2</sub> (Hardy <i>et al.</i> ) (Ref. 16)	100% D <sub>2</sub>	$m_0 = 172.15$			98.8	1.16
		$m_{\pm 1} = 174.75$		2.6		
		$m_{\pm 2} = 181.33$		6.58		

the disordered lattice at 4.1 K, with the asymmetry attributed to the short-range order of  $J = 1$  molecules. Similarly, the  $S_0(1)$  line was continuous and broad for the disordered lattice, but reduced to several resolvable modes for the ordered lattice. Their interpretation of the lines was disputed by Igarashi, who claimed the libron interaction leads to a different energy structure than Hardy *et al.* predicted.<sup>33</sup>

### 3. Heteronuclear molecules

The rotational Raman spectrum of the heteronuclear molecules HD and DT is different from the homonuclear

species. First, all heteronuclear molecules are in the  $J = 0$  state in the low temperature solid because the nuclei are distinguishable. Second, the measured  $S_0(0)$  line is broader for pure HD than either H<sub>2</sub> or D<sub>2</sub> with  $c(1) < 2\%$ . McTague *et al.*<sup>34</sup> showed that the HD  $S_0(0)$  line was composed of three polarization dependent peaks corresponding to the  $m_J$  states; however, the linewidth was about  $5 \text{ cm}^{-1}$  for each HD  $m_J$  state compared to  $0.6 \text{ cm}^{-1}$  for H<sub>2</sub>.<sup>30</sup> They attributed the linewidth to lifetime broadening due to the allowed  $\Delta J = 1$  transitions of the heteronuclear molecules.

### B. Review of vibrational raman spectra

The lowest vibrational transitions  $Q_1(J)$  are Raman active modes studied extensively over the years. The vibrational energies of the  $J = 0$  and  $J = 1$  molecules differ slightly due to the stretching of the  $J = 1$  molecules.<sup>8,30</sup> Additionally, the  $Q_1(0)$  and  $Q_1(1)$  energies both depend on  $c(1)$ ,<sup>3,35</sup> the solid density,<sup>9,36</sup> and the lattice.<sup>9,5,37</sup>

The  $Q_1(J)$  energy dependence on  $c(1)$  reveals the coupling of the molecular vibrational states. The frequency shift for both density and  $c(J)$  from the respective gas phase line is<sup>8,36,38,39</sup>

$$\Delta\nu(J) = \Delta\nu_0(J) - 6\epsilon \left( \frac{V_0}{V} \right)^2 c(J), \quad (10)$$

where  $V$  is the solid molar volume,  $V_0$  is the zero pressure solid molar volume, and  $\Delta\nu_0(J)$  is the single molecule coupling. The first term in Eq. (10) is due to the isotropic interactions in the solid and the second is the vibrational coupling term. Vibrational energy bands are formed by the coupling and allow the excitation to hop to neighboring molecules. However, the coupling is only between molecules with the same  $J$  because the energy difference  $\Delta Q_1 = Q_1(0) - Q_1(0)$  is nonzero.

The intensity of the  $Q_1(J)$  lines are strongly dependent on  $c(1)$  in pure  $H_2$  and  $D_2$ .<sup>3,8,38,39</sup> There is an enhanced intensity of the lower energy  $Q_1(1)$  line because, classically, the vibrating  $J = 1$  molecule drives neighboring  $J = 0$  molecules below their vibrational resonant frequency.<sup>2</sup> Thus, the  $Q_1(1)/Q_1(0)$  intensity ratio is described by

$$Q_1(1)/Q_1(0) = \xi[c(1)]c(1)/c(0), \quad (11)$$

where  $\xi[c(1)]$  is the concentration dependent enhancement factor.<sup>2,38</sup> James and Van Kranendonk initially used a coupled oscillator and interacting impurity model to calculate  $\xi[c(1)]$ .<sup>2</sup> The enhanced intensity was later successfully described by the coherent potential approximation.<sup>39</sup> Both models show that the small energy difference  $\Delta Q_1$  is responsible for  $\xi[c(1)] > 1$ . The  $D_2$  enhancement of about 50 is greater than the  $H_2$  value of about 4 for  $c(1) \approx 0$  because  $\Delta Q_1 = 3.5 \text{ cm}^{-1}$  for  $H_2$  compared to  $0.8 \text{ cm}^{-1}$  for  $D_2$  is smaller for  $D_2$  than  $H_2$ .<sup>2,38,40</sup>

Brown and Daniels<sup>9</sup> found that the vibrational transition was dependent on the isotope concentration for  $H_2$ -HD- $D_2$  mixtures. The transitions were shifted to higher energies as the  $H_2$  was diluted by the other isotopes by as much as 2% at about 300 kbar. Assuming that our hydrogen mixtures follow a simple scaling law, then  $H_2$  in the H-D experiences a lattice density equivalent to 200 bar.<sup>18</sup> Brown and Daniels measured almost no energy shift at this pressure.

### II. EXPERIMENT

Our samples consisted of a single D-T mixture and several compositions of  $H_2$ , HD, and  $D_2$ . The D-T sample was an 800  $\mu\text{m}$  diameter glass shell filled with 25 atm of D-T gas at room temperature, giving  $3 \times 10^{-7}$  moles of D-T. The experimentally determined D-T isotopic concentration was 29-51-20  $D_2$ -DT- $T_2$ . The shell was glued to a sapphire window

and mounted to the cold finger of a liquid helium cooled cryostat. The  $H_2$ , HD, and  $D_2$  mixtures were deposited directly on the sapphire window. Germanium resistance thermometers monitored the cell temperature and provided feedback for the temperature controller. Temperature variations were  $\pm 10$  mK over minutes, with slow drifts of up to  $\pm 200$  mK over the course of a day. The 488 nm line of a Spectra Physics 171  $\text{Ar}^+$  laser excited the sample. The back-scattered light was passed through a Kaiser Optical HSNF 488-1.0 holographic notch filter to remove the Rayleigh scattered light then dispersed by a Spex 1403 double monochromator. The spectrometer gratings were 1800 lines/mm blazed for 500 nm. The Raman signal was detected with a Princeton Instruments liquid nitrogen cooled CCD camera with a  $1152 \times 256$  array of  $22.5\text{-}\mu\text{m}$  square pixels.  $c(1)$  could not be determined below 4% in D-T because the  $S_0(1)$  signal was small compared to the CCD background noise.

The pure vapor phase  $D_2$   $S_0(0)$  transition was used to calibrate the optical system as it could be added around the D-T shell to provide an in-place calibration of the entire optical system. The spectrometer dispersion was found to be  $0.21 \text{ cm}^{-1}$  per pixel for the rotational lines and  $0.15 \text{ cm}^{-1}$  per pixel for the  $D_2$  vibrational lines. The maximum spectrometer entrance slit width was 35  $\mu\text{m}$ .

The solid was frozen quickly through the triple point and resulted in a randomly oriented multicrystalline sample.  $H_2$ , HD, and  $D_2$  were mixed in the vapor phase, then condensed onto the substrate. The solid pressure, temperature, and  $c(1)$  were such that the hcp phase is preferred for pure  $H_2$  or  $D_2$ . However, the lattice structure was not experimentally determined for the mixtures, nor could it be inferred from the  $S_0(0)$  line shape. Both  $c(1)$  and the isotope ratio was determined from the relative rotational line intensities according to Eq. (2).  $H_2$  and  $D_2$  samples with low  $c(1)$  were prepared by keeping the samples in liquid helium cooled storage beds. The  $J = 1$ -to-0 conversion took place over several weeks. It was previously shown that  $c(1)$  reaches a minimum value of 0.5-1% in D-T due to beta-particle interactions.<sup>41</sup>

### III. ROTATIONAL LINES

The rapid decay of the  $J = 1$  population in D-T enabled a measurement of the D-T  $S_0(0)$  line shapes with  $c(1)$ . The  $S_0(J)$  lines are easily identified for each hydrogen isotope based on their respective transition energies. Thus,  $c(1)_x$  and the  $S_0(0)$  lines for each isotope in the mixture are readily measured. Shortly after freezing, when a significant  $J = 1$  population exists, the  $D_2$ ,  $T_2$  and DT  $S_0(0)$  lines are broad and their respective  $m_J$  components cannot be resolved, as shown in the bottom trace of Fig. 1. This observation is consistent with previous measurements of the  $S_0(0)$  lines for pure component  $H_2$  and  $D_2$  with  $c(1) \geq 20\%$ .<sup>8,30</sup> The observed lineshapes for the D-T mixture at with  $c(1) \leq 15\%$  were not expected, and are very different from the single component results. Figure 1 shows the  $S_0(0)$  lines for  $T_2$ , DT, and  $D_2$  in D-T for decreasing  $c(1)$ . A triplet is evident for the  $T_2$   $S_0(0)$  line when  $c(1)_{T_2} < 10\%$ . However, the  $D_2$   $S_0(0)$  line remains broad and asymmetric for  $c(1)_{D_2} \leq 1$



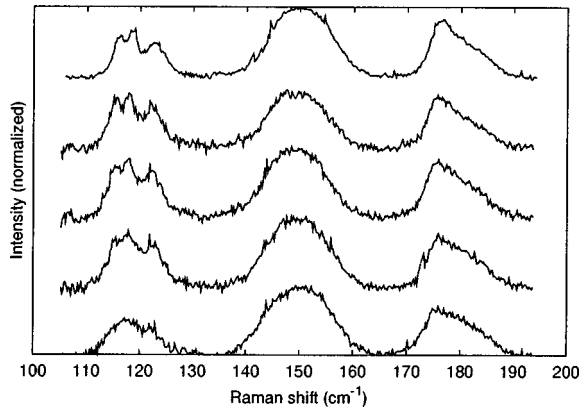


FIG. 1. The  $S_0(0)$  transitions in D-T for each isotope as the  $J = 1$  population decreases. The transitions correspond to (from left to right)  $T_2$ , DT, and  $D_2$  molecules. The  $T_2$  line shape is a triplet at the latest times, while the  $D_2$  retains the asymmetric shape. The time since cooling from 77 to 6.0 K is (bottom to top) 0.4, 3.0, 6.1, and 13.2 h. The top curve was measured after 77 h at 10 K.

–2%. The DT line is broad and nearly symmetric, similar to pure HD  $S_0(0)$  lines,<sup>34</sup> but with a few subtle differences that will be described shortly.

#### A. Comparison of the homonuclear isotope $S_0(0)$ transitions

$D_2$  was the common isotope in both the tritiated D-T and the nontritiated H-D mixtures. It is instructive to compare the  $D_2$   $S_0(0)$  line in both mixtures to  $S_0(0)$  of pure  $D_2$ . As previously described, the  $S_0(0)$   $m_J$  lines of  $J = 0$   $D_2$  are split into a triplet for hcp lattice and a doublet for fcc lattice, with the triplet structure resolved when  $c(1) \leq 20\%$ .<sup>30</sup> However, the  $D_2$   $S_0(0)$  triplet is not observed in D-T, even with  $c(1)$  less than 2–4%. Instead, the  $S_0(0)$  line has a full width at half maximum (FWHM) of  $9.0 \text{ cm}^{-1}$  and has a long, high energy tail when  $c(1) < 2-4\%$ . The low energy peak is less pronounced and the FWHM is  $11.5 \text{ cm}^{-1}$  with  $c(1)_{D_2} = 33\%$ . In contrast to  $D_2$ , the  $T_2$   $S_0(0)$  line did split into a triplet for  $c(1)_{T_2} < 10\%$ . However, the  $T_2$  triplet in D-T is not necessarily associated with the hcp lattice structure. Whereas the  $m_J$  splitting is the same to within  $0.02 \text{ cm}^{-1}$  for pure  $H_2$  and  $D_2$  samples,<sup>30,34</sup> the  $T_2$   $S_0(0)$  lines are 2.5 and  $3.9 \text{ cm}^{-1}$  below and above the center peak respectively.

The  $S_0(0)$  lines of  $H_2$ - $D_2$  mixtures with  $c(1) < 5\%$  are shown in Fig. 2. The  $D_2$   $S_0(0)$  line is split into the expected hcp triplet when no  $H_2$  is present. Adding  $H_2$  broadens the  $D_2$  line, with the triplet becoming unresolvable when the sample contains 23%  $H_2$ . A triplet is again resolvable when the  $D_2$  is strongly diluted by 77%  $H_2$ . Table I lists the peak positions and FWHM values for each of the  $S_0(0)$  components determined by fitting  $S_0(0)$  to a sum of Lorentzian lines. The FWHM of the  $D_2$   $m_J$  increase from  $1.0 \text{ cm}^{-1}$  for pure  $D_2$  to  $2.9 \text{ cm}^{-1}$  and  $2.5 \text{ cm}^{-1}$  with 12%  $H_2$ . There was little observed change in the splitting of the  $D_2$   $m_J$  components between the 0%  $H_2$  and 12%  $H_2$  samples. The  $D_2$   $S_0(0)$  line was again fit to the sum of three Lorentzian lines for 23%  $H_2$ , even though the individual lines could not be resolved, in order to obtain approximate positions and

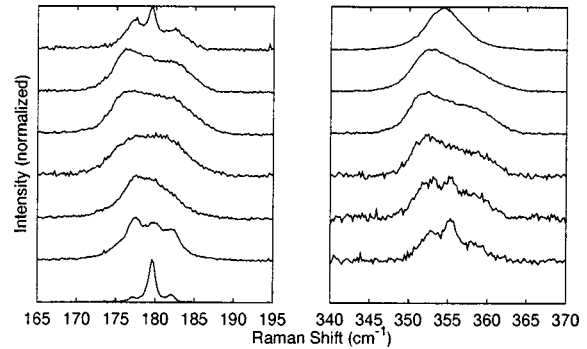


FIG. 2. The  $D_2$  (left) and  $H_2$  (right)  $S_0(0)$  transitions for increasing  $H_2$  concentration. The triplet structure of both isotopes is broadened as  $H_2$  is increased. The amount of  $H_2$  in the sample is (bottom to top) 0%, 12%, 23%, 31%, 45%, 59% and 77%.

FWHM values. While the FWHM of the  $D_2$   $S_0(0)$  components increases compared to the 0% and 12%  $H_2$  samples, the peak positions are not significantly shifted compared to the pure component. In contrast, the  $D_2$   $S_0(0)$  lines in the 77%  $H_2$ -23%  $D_2$  mixture are significantly shifted in energy compared to the samples with  $H_2 < 23\%$ .

Similarly, the  $H_2$   $S_0(0)$  line is composed of a triplet for the lowest concentrations of  $H_2$  in  $D_2$ , but the triplet becomes unresolvable between 23% and 31%  $H_2$ . The positions and FWHM values were again obtained by fitting to a sum of three Lorentzian lines, and are listed in Table I. As with  $D_2$  and  $T_2$ , the  $H_2$   $S_0(0)$   $m_J$  components are much broader in the mixture than for pure  $H_2$ .

Next, HD was added to the  $H_2$ - $D_2$  mixture. The  $D_2$   $S_0(0)$  triplet re-emerges, as shown in Fig. 3, but the lines are broad and significantly shifted in energy compared to pure  $D_2$ . The splitting of the three lines is not symmetric about the center energy, similar to the  $T_2$   $S_0(0)$  lines in D-T. The  $H_2$  lines do not show any evidence of a triplet, but instead have an asymmetric shape similar to that observed for  $D_2$  in D-T. Between each step, the gas was warmed up to the vapor to ensure mixing of the hydrogens. Hence, the crystal orientation, sizes, and number are likely very different from case to case. However, the lines are qualitatively similar in all cases.

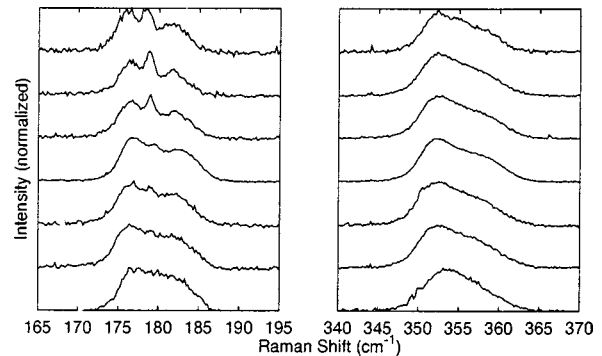


FIG. 3. The rotational lineshape for  $D_2$  (left) and  $H_2$  (right) as HD is added to the  $H_2$  and  $D_2$  mixture. The structure remains broad, but the triplet structure re-emerges. The percent of  $H_2$ -HD- $D_2$  is (bottom to top) 65-0-35, 55-11-34, 51-18-31, 45-27-28, 44-35-21, 46-38-16, and 29-51-20.

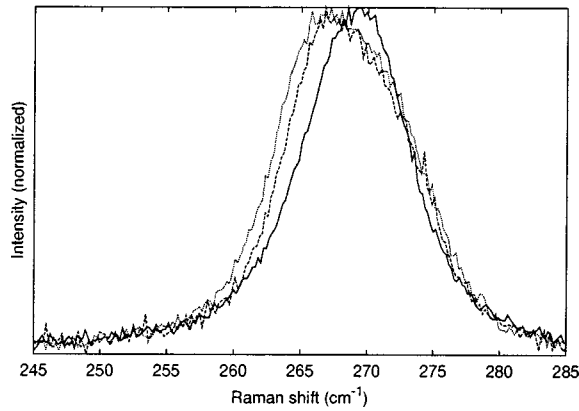


FIG. 4. The HD  $S_0(0)$  line for pure HD (solid) and the  $H_2$ -HD- $D_2$  mixtures 45-27-28 (dashed), and 29-51-20 (dotted). The linewidth is increased in the mixtures.

### B. $S_0(1)$ in D-T

The  $S_0(1)$  transition in D-T was measured for  $D_2$  and  $T_2$ . The  $S_0(1)$  line is at energy  $202.5 \text{ cm}^{-1}$  for  $T_2$  with a FWHM of  $7.5 \text{ cm}^{-1}$ . The  $S_0(1)$  line of  $D_2$  is at  $299.3 \text{ cm}^{-1}$  and has a FWHM of  $6.4 \text{ cm}^{-1}$ . No change in energy was observed with decreasing  $c(1)_{D_2}$  and  $c(1)_{T_2}$ . However, the  $D_2 S_0(1)$  becomes narrower with decreasing  $c(1)$ , with low intensity wings on each side of the main peak. The  $S_0(1)$  lines were not measured in the H-D samples because of the low  $J = 1$  population in those samples.

### C. $S_0(0)$ transitions of heteronuclear molecules

Figures 1 and 4 show the DT and HD  $S_0(0)$  lines in their respective mixtures. There is a qualitative similarity between the two isotopes. Both are broad, symmetric transitions, not too different from previous measurements of pure component HD. Neither HD nor DT have the strong line shape changes observed for the homonuclear molecules in the mixtures. Instead, only subtle differences were noticed.

The energies and FWHM values of the DT  $S_0(0)$  line as  $c(1)_{D_2}$  and  $c(1)_{T_2}$  decrease are listed in Table II. The FWHM increases slightly and the peak intensity shifts to higher energy as  $c(1)_{T_2}$  and  $c(1)_{D_2}$  increase. Similarly, the HD  $S_0(0)$  line is broadened and shifted to higher energy for HD in the H-D mixture compared to pure HD. Indeed, Fig. 5 shows that the  $S_0(0)$  lines of HD in H-D and DT in D-T are very nearly identical for comparable isotope ratios and  $c(1) < 5\%$ . McTague *et al.*<sup>34</sup> determined the HD  $S_0(0)$  line

TABLE II. Position and linewidth information of the DT  $S_0(0)$  line for the D-T mixture. The linewidth decreases with decreasing  $c(1)$  of  $D_2$  and  $T_2$ .

Time after cooling (hours)	Temp. (K)	% J = 1 ( $D_2, T_2$ )	Max ( $\text{cm}^{-1}$ )	Center ( $\text{cm}^{-1}$ )	FWHM ( $\text{cm}^{-1}$ )
0.75	11.0	(30,55)	150.9	150.7	13.5
25.5	11.0	(10,<5)	150.6	150.25	12.4
77.0	10.2	(<4,<4)	150.0	150.0	12.6

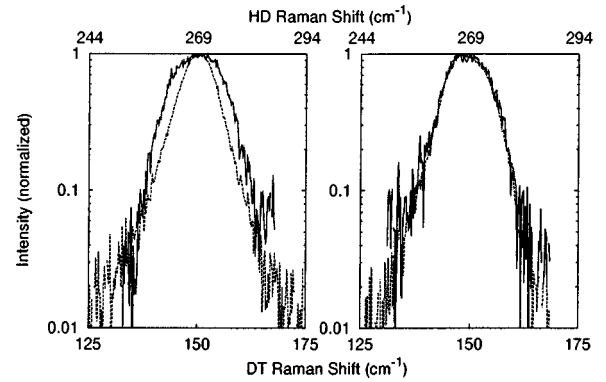


FIG. 5. The  $S_0(0)$  lines for HD (dashed) and DT (solid) overlaid. The left shows pure HD with no  $J = 1$  molecules and DT in D-T with  $c(1)_{T_2} = 55\%$  and  $c(1)_{D_2} = 30\%$ . The right shows HD in H-D and DT in D-T with  $c(1)_x < 5\%$ .

was composed of three  $m_J$  components that were each well fit by a Lorentzian line shape. Hence, they concluded that the width of the HD line was due to lifetime broadening. In contrast, HD in H-D and DT in D-T are both fit better by the sum of three Gaussian lines, suggesting that the broadening in the mixtures is due to the inhomogeneous crystalline environment.

### D. Rotational line shape discussion

The matrix of the mixtures differs from the single component case in three ways that alter the  $S_0(0)$  transitions. First, each isotope has a different rotational energy due to their differing masses. Second, the interaction potential varies slightly with the isotope. Finally, the lattice is distorted from the ideal hcp structure by the different sized molecular wave functions. The following discussion assumes only molecules in the  $\nu=0$  vibrational state on a rigid lattice.

The  $J = 2$  excitation of a  $D_2$  molecule cannot hop to a neighboring  $H_2$  molecule because the two have different rotational energies. Thus, the allowed rotational band states due to the EQQ interaction in a mixed hydrogen lattice are not the same as the single component case. New rotational states are accessible in the mixed lattice, and this broadens the  $S_0(0)$  transition. The crystal field terms of Eq. (7) are similarly altered, most notably for the distorted hcp lattice. While the small numbers of rotons in the lattice at any given time do not interact with each other, they each sample a different local lattice configuration. Hence, the measured  $S_0(0)$  line is an ensemble average of many different band energies. Thus the fact that the  $S_0(0)$  triplet broadens in mixtures of the hydrogens is not surprising. The origin of the  $S_0(0)$  triplet for the low concentration homonuclear isotope in H-D or D-T mixtures can also be explained in terms of the altered band energies, as described below.

The calculation in Sec. I A was modified to numerically model the mixed  $H_2$ - $D_2$  matrix with varying  $H_2$  concentration. Only the EQQ hopping interaction was calculated for the mixed lattice. In the model,  $H_2$  and  $D_2$  molecules are randomly placed, based on the desired  $H_2$  concentration, at specific lattice sites of a perfect lattice. The EQQ coupling

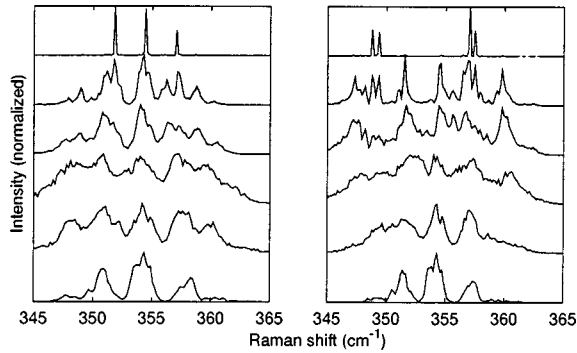


FIG. 6. Calculated spectrum for the  $S_0(0)$  line of  $H_2$  in an  $H_2$ - $D_2$  lattice for hcp (left) and fcc (right) lattice structures. The  $H_2$  concentrations are (bottom to top) 12%, 30%, 50%, 80%, 90%, and 100%.

strength  $\epsilon_{02}$  is dependent on the nearest neighbor distance, which was linearly interpolated from the pure  $D_2$  3.605-Å to the pure  $H_2$  3.789-Å values based on the  $H_2$  concentration. The lattice sum in Eq. (5) is taken only over lattice sites which have the same isotope as the molecule at the origin since the excitation cannot hop to molecules with difference  $S_0(0)$  energies. The energy eigenvalues are found by diagonalizing the resulting matrix in Eq. (3). The eigenvalues are then averaged for many randomly generated configurations to approximate the spectrum observed in a real crystal. The resulting spectra for  $H_2$  are presented, with  $D_2$  qualitatively the same. The polarization dependence of the intensity was neglected so that we report only the allowed energy spectrum. The interactions were calculated only to molecules within 5 nearest neighbors of the central molecule. Going further did not significantly alter the results for the cases tested.

The calculated  $H_2$   $S_0(0)$  spectra for the hcp and fcc lattices are shown in Fig. 6 for several  $H_2$  concentrations. Concentrations of less than about 5% (not shown) reduce to a single line with no energy shift from the free molecule value because there are, on average, no nearest neighbor pairs of  $H_2$  molecules. The hcp and fcc  $S_0(0)$  lines are split into nearly identical triplets at 12%  $H_2$  concentration. The  $S_0(0)$  transition remains broad for  $H_2$ , less than 90%, finally recovering the familiar hcp triplet and fcc doublet at 100%. The calculated spectrum will be further broadened by the crystal field terms. While the calculation does not exactly match the experiment, it does reproduce the more striking features. This indicates the  $|2m\rangle$  states are mixed in the  $H_2$ - $D_2$  lattice, and  $m$  is no longer a good quantum number. Therefore, the individual components of the  $T_2$  triplet in D-T and the  $D_2$  triplet in H-D are not designated by  $m_j$ . Including crystal field terms and distortions from the perfect lattice in the calculation will further modify the spectra, tending to broaden the transition, and will likely lead to the observed difference between  $\Delta_1$  and  $\Delta_2$ .

Thus, the  $S_0(0)$  triplet for hydrogen mixtures is not unique to the hcp lattice, and the crystal structure of the D-T and H-D mixtures remains uncertain. Furthermore, the H-D and D-T mixtures are qualitatively similar, hence there is no

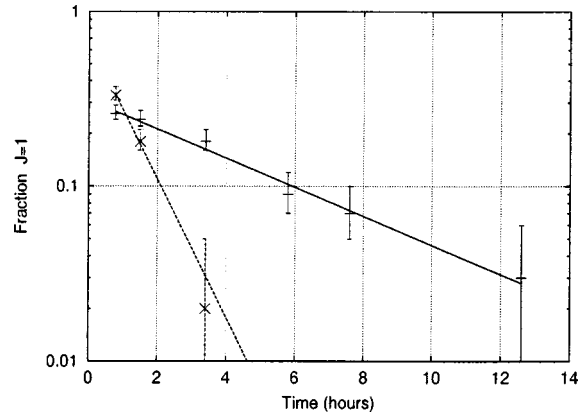


FIG. 7. Measured  $T_2$  ( $\times$ ) and  $D_2$  ( $+$ )  $c(1)$  vs time at 8.1 K. The  $J = 1$  concentrations for both isotopes decay exponentially. The straight lines are least squares fits to the data.

observable effect of radiation damage or free atoms on the rotons.

### E. $J = 1$ -to-0 conversion rates

The  $J=1$ -to-0 transition of  $H_2$  and  $D_2$  molecules is a second order process in  $c(1)$ . The magnetic dipole-dipole (and electric quadrupole-quadrupole for  $D_2$ ) interaction of neighboring  $J = 1$  molecules flips the spin of one of the nucleons with a simultaneous change in rotational state. The  $J = 1$ -to-0 conversion in D-T was found to be dominated by the atoms created by the tritium radioactivity.<sup>21,42-44</sup> The diffusion of atoms through the solid leads to a first order conversion rate in the D-T mixture. The very large electric field of the atoms and electrons created by the triton beta decay and subsequent ionization is responsible for the rapid conversion. Furthermore, the difference in conversion rates for  $D_2$  and  $T_2$  was attributed to their different magnetic moment, consistent with the theory. However, the NMR measurements were an indirect measure of the  $D_2$   $J = 1$  populations in the sample. The rotational Raman spectrum was used to obtain the relative number of molecules in each rotational state.

Figure 7 shows  $c(1)_x$  for  $T_2$  and  $D_2$ , determined according to Eq. (2), as a function of time at 8.1 K.  $c(1)_x$  decays exponentially in time for both isotopes, in agreement with the hopping model, and in contradiction to the second order process of natural conversion. Table IV shows the measured time constants at a series of temperatures. The typical error is  $\pm 0.3$  h for  $\tau(T_2)$  and 0.6 h for  $\tau(D_2)$ . The average  $\tau(D_2)/\tau(T_2)$  ratio is 3.7 h for all measurements between 5 and 10 K, in close agreement with the expected ratio of 3.47 based on the  $D_2$  and  $T_2$  magnetic moment ratios.

TABLE III. Position and linewidth information of the HD  $S_0(0)$  line for mixtures of HD,  $H_2$ , and  $D_2$ .

Sample	Temp. (K)	Max ( $\text{cm}^{-1}$ )	Center ( $\text{cm}^{-1}$ )	FWHM ( $\text{cm}^{-1}$ )
1-98-1	8.2	269.1	269.1	9.4
45-27-28	6.5	267.1	268.1	11.0
29-51-20	7.8	267.0	268.4	11.9

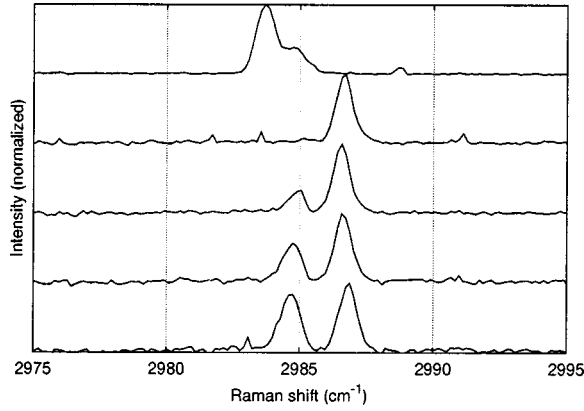


FIG. 8.  $Q_1(1)$  (left) and  $Q_1(0)$  (right) of  $D_2$  in D-T for  $c(1)_{D_2}$  (bottom to top) 30%, 19%, 10%, <2%. The top spectrum is pure  $D_2$  with 4%  $J=1$ . The sample temperature was 8.0 K.

IV. VIBRATIONAL LINES

The  $Q_1(0)$  and  $Q_1(1)$  Raman transitions were recorded for the isotopes in the D-T and H-D mixtures. The instrument resolution of  $\approx 0.16 \text{ cm}^{-1}/\text{pixel}$  is much larger than the vibron intrinsic FWHM of  $0.002 \text{ cm}^{-1}$  for  $c(1)=1.3\% \text{ H}_2$ .<sup>39</sup> Vapor and solid phase  $D_2$   $Q_1(J)$  lines with  $c(1)<1\%$  served to calibrate the spectrometer energies. Thus, the relative energy shifts and difference  $\Delta Q_1=Q_1(0)-Q_1(1)$  are known more accurately than the absolute energies, especially for  $H_2$  and  $T_2$ .  $Q_1(J)$  energies and intensities were obtained by fitting the measured lines to a Gaussian function.

A.  $Q_1(J)$  energies in D-T and H-D mixtures

Figures 8 and 9 show typical  $D_2$  and  $T_2$   $Q_1(J)$  transitions in D-T.  $Q_1(0)$  is the higher energy line in each of the figures.  $c(1)_{T_2}$  and  $c(1)_{D_2}$  were calculated using the time constants obtained in Table III. The  $T_2$  time constant is shorter than  $D_2$ , thus the observed changes in the  $T_2$   $Q_1(J)$  are not strongly influenced by  $c(1)_{D_2}$ , and vice versa.  $\Delta Q_1$  is small for both  $D_2$  and  $T_2$  and in many cases at the limit of our resolution.  $\Delta Q_1$  decreases with decreasing  $c(1)_x$  for both  $D_2$

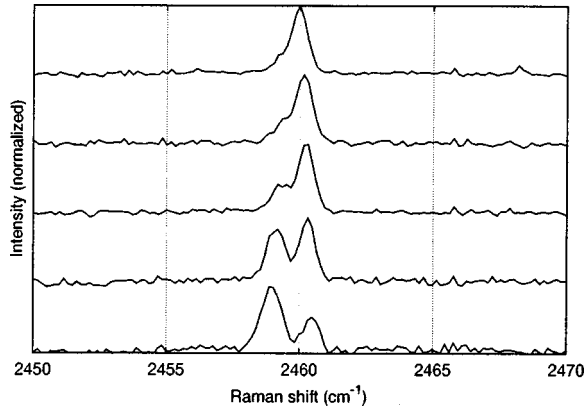


FIG. 9.  $Q_1(1)$  (left) and  $Q_1(0)$  (right) of  $T_2$  in D-T for  $c(1)_{T_2}$  (bottom to top) 50%, 23%, 8%, 3%, <1%. The sample temperature was 8.0 K.

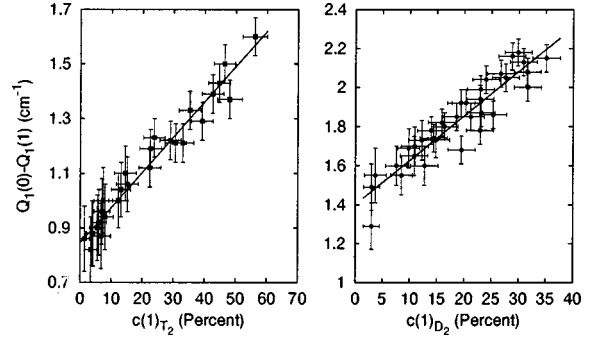


FIG. 10. Energy difference  $\Delta Q_1$  for  $T_2$  (left) and  $D_2$  (right) in D-T as a function of  $c(1)$ . The separation decreases as  $J = 1$  decreases. The straight lines are linear least square fits to the data described in the text.

and  $T_2$ , shown in Fig. 10. The straight lines in the figure are linear least squares fits to the data, with

$$\Delta Q_1 = \begin{Bmatrix} 0.84 + 0.013c(1)_{T_2} & T_2 \\ 1.40 + 0.023c(1)_{D_2} & D_2 \end{Bmatrix}. \quad (12)$$

$\Delta Q_1$  is smaller for  $T_2$  than  $D_2$  at a given  $c(1)_x$ , consistent with the isotope change previously observed with  $D_2$  and  $H_2$ .<sup>3,39,40</sup> Figure 8 includes the  $Q_1(J)$  lines in pure  $D_2$  with  $c(1)_{D_2} \approx 4\%$ , and shows that the  $D_2$   $Q_1(0)$  line is shifted higher by  $1.9 \text{ cm}^{-1}$  in D-T with low  $c(1)_{D_2}$  than in pure  $D_2$ . Similarly,  $\Delta Q_1$  is larger for  $D_2$  in D-T than for pure  $D_2$ .

Corresponding shifts in the  $D_2$   $Q_1(J)$  energies were found as  $H_2$  and  $D_2$  were mixed as shown in Fig. 11.  $c(1)_{D_2} = 4\%$  and  $c(1)_{H_2} = 6\%$  for each plot in Fig. 11. The  $Q_1(J)$  energies are plotted in Fig. 12 as a function of  $D_2$  concentration, where the mixture included HD for points with less than 39%  $D_2$ . The linear fits in Fig. 12 are

$$\begin{aligned} Q_1(0) &= 2987.5 - 0.027c_{D_2} \\ Q_1(1) &= 2985.8 - 0.015c_{D_2}. \end{aligned} \quad (13)$$

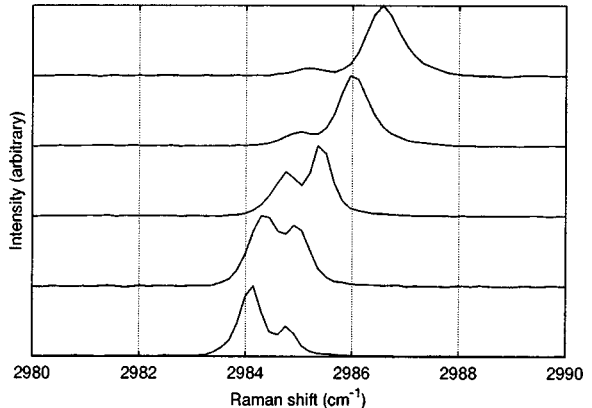


FIG. 11. The  $D_2$  vibrational spectrum as  $H_2$  is mixed with  $D_2$ . The amount of  $H_2$  is (bottom to top) 0%, 12%, 31%, 45%, and 59%.  $c(1)_{D_2} < 5\%$ .



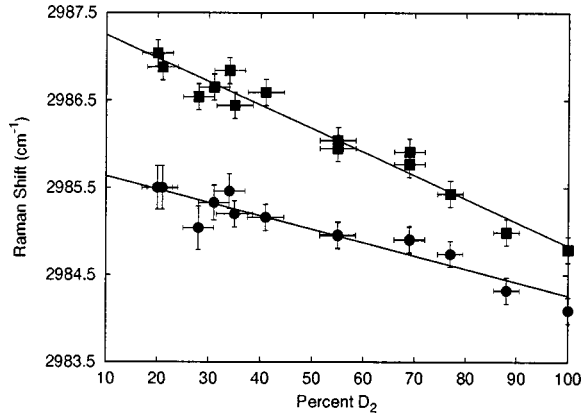


FIG. 12. The energy shift of the D<sub>2</sub> Q<sub>1</sub>(1) (●) and Q<sub>1</sub>(0) (■) as H<sub>2</sub> and HD are added.

The fits do not depend on whether the mixture is H<sub>2</sub>-D<sub>2</sub> or H<sub>2</sub>-HD-D<sub>2</sub>. Furthermore, the D<sub>2</sub> Q<sub>1</sub>(J) lines in H-D are at nearly the same energy for equivalent  $c(1)_{D_2}$  and D<sub>2</sub> concentrations in D-T. Thus, the energy shift of D<sub>2</sub> Q<sub>1</sub>(J) lines depends only on the D<sub>2</sub> concentration and not on the components of the mixture.

The H<sub>2</sub> lines were recorded with the addition of HD to the mixture. A small increase of  $\Delta Q_1 = 4.66 \text{ cm}^{-1}$  to  $5.00 \text{ cm}^{-1}$  was found when the H<sub>2</sub> concentration decreased from 65% to 44%. The H<sub>2</sub> Q<sub>1</sub>(1) line consisted of a doublet separated by  $0.5 \text{ cm}^{-1}$  in energy, previously attributed to clustering of J = 1 molecules.<sup>38</sup>

### B. Q<sub>1</sub>(1)/Q<sub>1</sub>(0) intensity ratio in D-T and H-D

Figure 13 shows the measured Q<sub>1</sub>(1) to Q<sub>1</sub>(0) intensity ratio for two cases. The first shows the increase of Q<sub>1</sub>(1)/Q<sub>1</sub>(0) with  $c(1)_x$  for D<sub>2</sub> and T<sub>2</sub> in D-T. The fit functions are

$$Q_1(1)/Q_1(0) = \left\{ \begin{array}{l} 2.19 \frac{c(1)_{T_2}}{100 - c(1)_{T_2}} + 0.28 \quad T_2 \\ 2.29 \frac{c(1)_{D_2}}{100 - c(1)_{D_2}} \quad D_2 \end{array} \right. \quad (14)$$

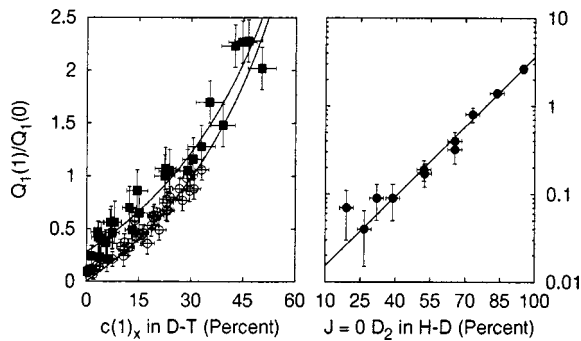


FIG. 13. Ratio of the Q<sub>1</sub>(1) to Q<sub>1</sub>(0) intensities. Left is for T<sub>2</sub> vs  $c(1)_{T_2}$  (squares) and D<sub>2</sub> vs  $c(1)_{D_2}$  (open circles) in D-T. Right is D<sub>2</sub> concentration (solid circles) of the H<sub>2</sub>-HD-D<sub>2</sub> mixture. The lines are fits to the data as described in the text.

The first term is the concentration ratio multiplied by the enhancement factor,  $\xi$  in Eq. (11). Thus, the intensity ratio is enhanced by more than a factor of two for both D<sub>2</sub> and T<sub>2</sub> in the D-T mixture. The fit does not pass through the origin for T<sub>2</sub> which may indicate the calculated  $c(1)_{T_2}$  is low by 3–4%.

The second plot in Fig. 13 shows an exponential increase of the intensity ratio with D<sub>2</sub> concentration in the H-D mixture with  $c(1)_{D_2} = 4\%$ . The fit function is

$$Q_1(1)/Q_1(0) = 8.4 \times 10^{-3} \exp[c(1)_{D_2}/16.5]. \quad (15)$$

These results show that  $\xi$  is slightly higher for D<sub>2</sub> in D-T than D<sub>2</sub> in H-D under equivalent conditions. Both mixtures have  $\xi$ 's for D<sub>2</sub> which are much lower than is found in the pure component for a given  $c(1)_{D_2}$ .

### C. Discussion

A common point in both D-T and H-D mixtures is when they each have 30% D<sub>2</sub> and  $c(1)_{D_2} \approx 5\%$ . The D<sub>2</sub> Q<sub>1</sub>(0) line is at  $2986.7 \text{ cm}^{-1}$  in both mixtures, while the Q<sub>1</sub>(1) line is at  $2985.2 \text{ cm}^{-1}$  in D-T and  $2985.35 \text{ cm}^{-1}$  in H-D. Both lines are shifted substantially from the pure D<sub>2</sub> with  $c(1)_{D_2} = 5\%$  values of  $Q_1(0) = 2984.8 \text{ cm}^{-1}$  and  $Q_1(1) = 2983.7 \text{ cm}^{-1}$ . It is important to note that the solid density is lower (higher) for H-D (D-T) than D<sub>2</sub> at zero pressure and equivalent temperatures. Rather, the energy shift depends only on the D<sub>2</sub> concentration. The Q<sub>1</sub>(0) shift with increasing impurity concentration is consistent with Eq. (10) where  $c(J=0)$  is replaced by the D<sub>2</sub> concentration. The predicted shift for D<sub>2</sub> Q<sub>1</sub>(0) is  $1.6 \text{ cm}^{-1}$  using  $6\epsilon = 2.2 \text{ cm}^{-1}$  with 30% D<sub>2</sub>, close to the  $1.9 \text{ cm}^{-1}$  found in the experiment. In contrast, Q<sub>1</sub>(1) is not expected to shift appreciably with the addition of H<sub>2</sub> and HD based on Eq. (10). The absolute D<sub>2</sub> J = 1 concentration decreases from 4% to 1.2% when D<sub>2</sub> is diluted to 30% of the sample. The initial sample with  $c(1)_{D_2} = 4\%$  would show an energy increase of  $0.1 \text{ cm}^{-1}$  using Eq. (10) instead, of the  $1.05 \text{ cm}^{-1}$  actually measured.

Clustering of J = 1 molecules<sup>38</sup> is one possible explanation for the Q<sub>1</sub>(1) line shift. However, the J = 1 molecules in the initial sample had on average 0.5 J = 1 nearest neighbors, and should be dominated by clusters of number  $n=0$  and 1. The energy difference of the  $n=0$  and 1 clusters needs to be about  $1 \text{ cm}^{-1}$  to explain the data, larger than the  $0.4 \text{ cm}^{-1}$  found for H<sub>2</sub> (Ref. 38) and  $0.2 \text{ cm}^{-1}$  for D<sub>2</sub>.<sup>40</sup> Furthermore, a splitting of the required magnitude is not found for D<sub>2</sub> in D-T for any  $c(1)_{D_2}$  value. While clustering likely exists, the individual components cannot be resolved in the data.

The dependence on D<sub>2</sub> concentration but not the other isotopes suggests that reduced lattice symmetry is responsible for the vibron energy shift. The vibrons cannot hop between different isotopes, thus altering the band states of the crystal and shifting the Q<sub>1</sub>(J) lines.<sup>45</sup> This explanation is supported by a comparison with liquid D<sub>2</sub>. Bhatnagar *et al.* found that the Q<sub>1</sub>(1) and Q<sub>1</sub>(0) lines in liquid D<sub>2</sub> are higher by  $1.7$  and  $1.4 \text{ cm}^{-1}$ , respectively, compared to the solid.<sup>30</sup>

TABLE IV. Measured  $1/e$  times for  $T_2$  and  $D_2$   $J=1 \rightarrow 0$  in this experiment.

Temp. (K)	$\tau(T_2)$ (hours)	$\tau(D_2)$ (hours)	$\tau(D_2)/\tau(T_2)$
5.4	6.1	9.1	1.5
5.4	1.5	5.3	3.5
5.8	1.7	5.9	3.5
6.0	2.8	9.1	3.2
6.7	2.4	5.3	2.2
7.2	2.2	8.3	3.8
7.2	2.4	6.8	2.8
7.2	1.5	6.9	4.6
8.1	1.1	5.2	4.7
8.2	1.9	6.1	3.2
8.6		7.5	
8.7	1.5	7.3	4.9
9.3	2.0	8.8	4.4
9.6	2.2	6.2	2.8
9.6	1.9	7.8	4.1
10.2	1.1	7.6	6.9
10.2	1.8	8.8	4.9
10.2		5.8	
10.8	1.1	15.5	14
11.3	3.3	22	6.6
11.7	5.3	30	5.7

The magnitude of the shift is consistent with our measurement, even though their data was for  $c(1)_{D_2}=20\%$ .

The coupling of the  $J = 1$  and  $0$  vibrons leads to the enhanced  $Q_1(1)/Q_1(0)$  ratio in the hydrogens, as discussed in Sec. I B, compared to the  $c(1)/c(0)$  ratio.  $\xi$  is less in the D-T and H-D mixtures than in the pure components. The coupling between different isotopes is very weak because of the very large energy difference between their vibrational states.<sup>2,39,40</sup> Thus,  $\xi$  is reduced in mixtures because there are fewer neighboring molecules with strong coupling (see Tables IV and V).

## V. CONCLUSIONS

Rotational and vibrational Raman spectra of hydrogen mixtures are very different from the pure components. Both rotors and vibrons are localized in the mixture by the isotopic energy difference of the respective transitions. The well

TABLE V. Measured  $Q_1(0)$  and  $Q_1(1)$  line positions for  $H_2$ ,  $D_2$ , and  $T_2$ .

Species	Temp. (K)	$Q_1(0)$ ( $cm^{-1}$ )	$Q_1(1)$ ( $cm^{-1}$ )	$\Delta Q_1$ ( $cm^{-1}$ )
$H_2$ in 75 % $J = 1$ $H_2$ solid	8.2	4151.5	4142.8	8.7
44-35-21 $H_2$ -HD- $D_2$	7.2	4150.2	4145.2	5.0
65-0-35 $H_2$ -HD- $D_2$	8.5	4149.6	4145.0	4.6
$D_2$ in $D_2$ vapor <1% $J=1$	25	2993.5		
$D_2$ in 5% $J = 1$ $D_2$ solid	8	2984.8	2983.7	1.1
$D_2$ in <1% $J = 1$ $D_2$ solid	12.7	2984.8	2984.1	0.7
$D_2$ in 30% $J = 1$ D-T solid	8	2986.9	2984.7	2.2
$D_2$ in $J = 0$ D-T solid	8	2986.7	2985.2	1.5
$D_2$ in $J = 0$ 59% $H_2$	9.5	2986.6	2985.4	1.2
$D_2$ in $J = 0$ 31% $H_2$	8	2985.4	2984.8	0.6
$D_2$ in $J = 0$ 12% $H_2$	9	2984.9	2984.3	0.6
$T_2$ in 50% $J = 1$ D-T solid	8	2460.5	2458.9	1.6
$T_2$ in $J = 0$ D-T solid	8	2460.0	2459.2	0.8

defined spatial symmetry of the hcp lattice is lost and the  $S_0(0)$   $m_J$  states are broadened into a continuous band. Thus, the hcp and fcc lattices cannot be distinguished in mixtures using the Raman spectra, as can be done with pure components. The vibron localization in mixtures increases the  $Q_1(J)$  energy in the solid mixtures by nearly the same amount observed in the pure-component liquid. Similarly, the  $Q_1(1)/Q_1(0)$  intensity enhancement for a given isotope is reduced in the mixtures compared to the pure component.

$D_2$  was common to all mixtures studied and showed that the  $S_0(0)$  and  $Q_1(J)$  spectra were nearly identical in H-D and D-T with similar  $D_2$  and  $J = 1$  concentrations. The spectra depend only on the  $D_2$  concentration, not the other components of the mixture. Finally, neither the  $S_0(J)$  nor the  $Q_1(J)$  lines appear to be effected by radiation damage in our D-T sample. The D-T lines are qualitatively similar to the H-D lines, and appear to depend on the mixture concentration, but not the actual impurity molecules in the mixture. The only radiation effect was the previously observed enhanced  $J = 1$ -to-0 conversion rate.

## ACKNOWLEDGMENTS

This work was performed under the auspices of the U.S. Department of Energy by the University of California, Lawrence Livermore National Laboratory under Contract No. W-7405-Eng-48.

<sup>1</sup>J. V. Kranendonk and V. F. Sears, Can. J. Phys. **44**, 313 (1966).

<sup>2</sup>H. M. James and J. V. Kranendonk, Phys. Rev. **164**, 1159 (1967).

<sup>3</sup>W. R. C. Prior and E. J. Allin, Can. J. Phys. **50**, 1471 (1972).

<sup>4</sup>W. R. C. Prior and E. J. Allin, Can. J. Phys. **51**, 405 (1973).

<sup>5</sup>M. E. Alikhani, B. Silvi, J. P. Perchard, and V. Chandrasekharan, J. Chem. Phys. **90**, 5221 (1989).

<sup>6</sup>V. Chandrasekharan, M. Chergui, B. Silvi, and R. D. Ethers, J. Phys. Chem. **91**, 1623 (1987).

<sup>7</sup>B. Silvi, V. Chandrasekharan, M. Chergui, and R. D. Ethers, Phys. Rev. B **33**, 2749 (1986).

<sup>8</sup>J. V. Kranendonk, *Solid Hydrogen* (Plenum Press, New York, 1983).

<sup>9</sup>D. M. Brown and W. B. Daniels, Phys. Rev. A **45**, 6429 (1992).

<sup>10</sup>I. F. Silvera and R. J. Wijngaarden, Phys. Rev. Lett. **47**, 39 (1981).

<sup>11</sup>F. Moshary, N. H. Chen, and I. F. Silvera, Phys. Rev. B **48**,

- 12 613 (1993).
- <sup>12</sup>J. V. Kranendonk, *Can. J. Phys.* **38**, 240 (1960).
- <sup>13</sup>I. F. Silvera, *Rev. Mod. Phys.* **52**, 393 (1980).
- <sup>14</sup>J. Lindl, *Phys. Plasmas* **2**, 3933 (1995).
- <sup>15</sup>K. Veirs, Tech. Rep. LBL-20565, Lawrence Berkeley Laboratory, 1985.
- <sup>16</sup>W. N. Hardy, I. F. Silvera, and J. P. McTague, *Phys. Rev. B* **12**, 753 (1975).
- <sup>17</sup>M. C. Drake, G. J. Rosasco, R. Schneggenburger, and R. L. Nolen, Jr., *J. Appl. Phys.* **50**, 7894 (1979).
- <sup>18</sup>P. C. Souers, *Hydrogen Properties for Fusion Energy* (University of California Press, Berkeley, 1986).
- <sup>19</sup>G. W. Collins, P. C. Souers, J. L. Maienschein, E. R. Mapoles, and J. R. Gaines, *Phys. Rev. B* **45**, 549 (1992).
- <sup>20</sup>J. R. Gaines, P. A. Fedders, G. W. Collins, J. D. Sater, and P. C. Souers, *Phys. Rev. B* **52**, 7243 (1995).
- <sup>21</sup>J. D. Sater, J. R. Gaines, E. M. Fearon, P. C. Souers, F. E. McMurphy, and E. R. Mapoles, *Phys. Rev. B* **37**, 1482 (1988).
- <sup>22</sup>J. J. Miller, R. L. Brooks, and J. L. Hunt, *Can. J. Phys.* **71**, 501 (1993).
- <sup>23</sup>K. Motizuki and T. Nagamiya, *J. Phys. Soc. Jpn.* **11**, 93 (1956).
- <sup>24</sup>K. Motizuki, *J. Phys. Soc. Jpn.* **12**, 1192 (1962).
- <sup>25</sup>J. A. Berlinsky and W. N. Hardy, *Phys. Rev. B* **8**, 5013 (1973).
- <sup>26</sup>W. Kolos and L. Wolniewicz, *J. Chem. Phys.* **46**, 1426 (1968).
- <sup>27</sup>C. Schwartz and R. J. Le Roy, *J. Mol. Spectrosc.* **121**, 420 (1987).
- <sup>28</sup>S. C. Durana and J. P. McTague, *Phys. Rev. Lett.* **31**, 990 (1973).
- <sup>29</sup>J. V. Kranendonk and G. Karl, *Rev. Mod. Phys.* **40**, 531 (1968).
- <sup>30</sup>S. S. Bhatnagar, E. J. Allin, and H. L. Welsh, *Can. J. Phys.* **40**, 9 (1962).
- <sup>31</sup>E. Goovaerts, X. Y. Chen, A. Bouwen, and D. Schoemaker, *Phys. Rev. Lett.* **57**, 479 (1986).
- <sup>32</sup>M. Leblans, A. Bouwen, C. Sierens, W. Joosen, E. Goovaerts, and D. Schoemaker, *Phys. Rev. B* **40**, 6674 (1989).
- <sup>33</sup>J. Igarashi, *Prog. Theor. Phys.* **61**, 719 (1979).
- <sup>34</sup>J. P. McTague, I. F. Silvera, and W. N. Hardy, in *Light Scattering in Solids: Proceedings of the Second International Conference on Light Scattering in Solids*, edited by M. Balkanski (Flammarion Sciences, Paris, 1971), pp. 456–459.
- <sup>35</sup>W. R. C. Prior and E. J. Allin, *Can. J. Phys.* **51**, 1935 (1973).
- <sup>36</sup>E. J. Allin and S. M. Till, *Can. J. Phys.* **57**, 442 (1979).
- <sup>37</sup>H. Kreek and R. J. Le Roy, *J. Chem. Phys.* **63**, 338 (1975).
- <sup>38</sup>V. Soots, E. J. Allin, and H. L. Welsh, *Can. J. Phys.* **43**, 1985 (1965).
- <sup>39</sup>J. De Kinder, A. Bouwen, D. Schoemaker, A. Boukahil, and D. L. Huber, *Phys. Rev. B* **49**, 12 754 (1994).
- <sup>40</sup>J. De Kinder, A. Bouwen, D. Schoemaker, A. Boukahil, and D. L. Huber, *Phys. Rev. B* **49**, 12 762 (1994).
- <sup>41</sup>G. W. Collins, P. C. Souers, J. L. Maienschein, E. R. Mapoles, and J. R. Gaines, *Phys. Rev. B* **45**, 549 (1992).
- <sup>42</sup>Y. Cao, J. R. Gaines, P. A. Fedders, and P. C. Souers, *Phys. Rev. B* **37**, 1474 (1988).
- <sup>43</sup>G. W. Collins, E. M. Fearon, E. R. Mapoles, R. T. Tsugawa, P. C. Souers, and P. A. Fedders, *Phys. Rev. B* **44**, 6598 (1991).
- <sup>44</sup>G. W. Collins, E. M. Fearon, E. R. Mapoles, R. T. Tsugawa, P. C. Souers, and P. A. Fedders, *Phys. Rev. B* **46**, 695 (1992).
- <sup>45</sup>J. L. Feldman, J. H. Eggert, J. De Kinder, H. K. Mao, and R. J. Hemley, *J. Low Temp. Phys.* **115**, 181 (1999).